










## Gynaecology

# Artificial intelligence-based tissue segmentation and cell identification in multiplex-stained histological endometriosis sections

Scott E. Korman <sup>1</sup>, Guus Vissers <sup>2</sup>, Mark A.J. Gorris <sup>1,3</sup>, Kiek Verrijp<sup>1,4</sup>, Wouter P.R. Verdurmen <sup>1</sup>, Michiel Simons <sup>4</sup>, Sebastien Taurin <sup>5</sup>, Mai Sater <sup>6</sup>, Annemiek W. Nap <sup>2,\*</sup>, and Roland Brock <sup>1,6,\*</sup>

<sup>1</sup>Department of Medical BioSciences, Radboudumc, Nijmegen, The Netherlands

<sup>2</sup>Department of Obstetrics and Gynaecology, Radboudumc, Nijmegen, The Netherlands



<sup>3</sup>Division of Immunotherapy, Oncode Institute, Radboud University Medical Center, Nijmegen, The Netherlands

<sup>4</sup>Department of Pathology, Radboudumc, Nijmegen, The Netherlands

<sup>5</sup>Department of Molecular Medicine, Arabian Gulf University, Manama, Kingdom of Bahrain

<sup>6</sup>Department of Medical Biochemistry, Arabian Gulf University, Manama, Kingdom of Bahrain

\*Correspondence address. Department of Obstetrics and Gynaecology, Radboud University Medical Center, PO Box 9101, 6500 HB Nijmegen, The Netherlands.

E-mail: annemiek.nap@radboudumc.nl  <https://orcid.org/0000-0002-2716-8351> (A.W.N.); Department of Medical BioSciences, Radboud University Medical Center, PO Box 9101, 6500 HB Nijmegen, The Netherlands. E-mail: roland.brock@radboudumc.nl  <https://orcid.org/0000-0003-1395-6127> (R.B.)

## ABSTRACT

**STUDY QUESTION:** How can we best achieve tissue segmentation and cell counting of multichannel-stained endometriosis sections to understand tissue composition?

**SUMMARY ANSWER:** A combination of a machine learning-based tissue analysis software for tissue segmentation and a deep learning-based algorithm for segmentation-independent cell identification shows strong performance on the automated histological analysis of endometriosis sections.

**WHAT IS KNOWN ALREADY:** Endometriosis is characterized by the complex interplay of various cell types and exhibits great variation between patients and endometriosis subtypes.

**STUDY DESIGN, SIZE, DURATION:** Endometriosis tissue samples of eight patients of different subtypes were obtained during surgery.

**PARTICIPANTS/MATERIALS, SETTING, METHODS:** Endometriosis tissue was formalin-fixed and paraffin-embedded before sectioning and staining by (multiplex) immunohistochemistry. A 6-plex immunofluorescence panel in combination with a nuclear stain was established following a standardized protocol. This panel enabled the distinction of different tissue structures and dividing cells. Artificial intelligence-based tissue and cell phenotyping were employed to automatically segment the various tissue structures and extract quantitative features.

**MAIN RESULTS AND THE ROLE OF CHANCE:** An endometriosis-specific multiplex panel comprised of PanCK, CD10,  $\alpha$ -SMA, calretinin, CD45, Ki67, and DAPI enabled the distinction of tissue structures in endometriosis. Whereas a machine learning approach enabled a reliable segmentation of tissue substructure, for cell identification, the segmentation-free deep learning-based algorithm was superior.

**LIMITATIONS, REASONS FOR CAUTION:** The present analysis was conducted on a limited number of samples for method establishment. For further refinement, quantification of collagen-rich cell-free areas should be included which could further enhance the assessment of the extent of fibrotic changes. Moreover, the method should be applied to a larger number of samples to delineate subtype-specific differences.

**WIDER IMPLICATIONS OF THE FINDINGS:** We demonstrate the great potential of combining multiplex staining and cell phenotyping for endometriosis research. The optimization procedure of the multiplex panel was transferred from a cancer-related project, demonstrating the robustness of the procedure beyond the cancer context. This panel can be employed for larger batch analyses. Furthermore, we demonstrate that the deep learning-based approach is capable of performing cell phenotyping on tissue types that were not part of the training set underlining the potential of the method for heterogenous endometriosis samples.

**STUDY FUNDING/COMPETING INTEREST(S):** All funding was provided through departmental funds. The authors declare no competing interests.

**TRIAL REGISTRATION NUMBER:** N/A.

**Keywords:** artificial intelligence / endometriosis / supervised machine learning / computer-assisted image analysis / multiplex immunofluorescence / 3,3'-diaminobenzidine / cell proliferation / fibrosis / inflammation

Received: June 9, 2024. Revised: October 17, 2024. Editorial decision: November 25, 2024.

© The Author(s) 2024. Published by Oxford University Press on behalf of European Society of Human Reproduction and Embryology.

This is an Open Access article distributed under the terms of the Creative Commons Attribution-NonCommercial License (<https://creativecommons.org/licenses/by-nc/4.0/>), which permits non-commercial re-use, distribution, and reproduction in any medium, provided the original work is properly cited. For commercial re-use, please contact [reprints@oup.com](mailto:reprints@oup.com) for reprints and translation rights for reprints. All other permissions can be obtained through our RightsLink service via the Permissions link on the article page on our site—for further information please contact [journals.permissions@oup.com](mailto:journals.permissions@oup.com).

## Introduction

Endometriosis is a gynaecological condition that casts a heavy burden on the health-related quality of life of individual patients, as well as our society. Although affecting around 1 in 10 women of childbearing age, it has historically lacked appropriate attention in research and clinical practice. Possible symptoms include dysmenorrhea, pelvic pain, and infertility (Horne and Missmer, 2022). Current treatment options are limited to contraceptive hormone therapy, pain and inflammation management, and surgical excision. However, these interventions are often unsatisfying as they only address the symptoms and are mostly incompatible with a wish to conceive (Kalaitzopoulos et al., 2021).

Endometriosis is defined by the presence of functioning implants of epithelial and stromal cells outside the uterine cavity, which closely resemble uterine endometrium. These lesions are generally divided into three categories based on their location. Superficial peritoneal lesions (PE) are found on the peritoneal surface epithelium. Deep lesions (DE) infiltrate fibromuscular tissue and are defined by a depth of >5 mm. Endometrioma (OMA) present as ovarian cysts that are often filled with tar-like fluid containing debris. In addition, there are anecdotal reports of endometriosis affecting the lungs or skin (Machairiotis et al., 2013; Raffi et al., 2019).

To this point, the pathological examination of endometriosis focuses on the macroscopic aspect of lesions, such as their location, and the histopathology including confirmation of endometrial stroma, endometrial glands, signs of haemorrhage, and exclusion of rare (pre)malignant changes. However, this approach neglects that not only with respect to localization but also with respect to the cellular level, endometriosis is highly heterogeneous (Colgrave et al., 2021). Besides epithelial and stromal cells, endometriotic lesions usually comprise myofibroblasts, mesothelial cells, and a variety of subsets of myeloid and lymphoid cells (Tan et al., 2022). Furthermore, lesions trigger neovascularization (Laschke and Menger, 2018; Chung and Han, 2022) and neurogenesis (Asante and Taylor, 2011). In these aspects, endometriotic lesions share many characteristics with tumours and their cellular microenvironment. Arguably, a better understanding of the heterogeneity and how it relates to disease progression, symptoms and therapy response may improve the clinical management of the disease and promote the development of new therapeutic options.

In cancer, multiplex immunohistochemistry (IHC) in combination with machine learning-based image analysis approaches is increasingly employed to investigate the spatial interplay of cell types (Gorris et al., 2022; Rojas et al., 2022; van Dam et al., 2022; Zidane et al., 2023). By comparison, in endometriosis, the use of multiplex IHC in combination with advanced cell image analysis protocols is still in its infancy. Recently, McKinnon et al. (2022) used the open-source software QuPath to quantify epithelial and stromal cells in endometriotic lesions stained by conventional IHC. The study by Tan et al. (2022) used imaging mass cytometry to visualize the composition of stromal, epithelial, and immune cells in several lesions, but without further computer-aided image analysis.

Machine learning algorithms reach their limits of accurately identifying individual cells in tissues with high cell density, which is frequently found in an inflammatory context. The abovementioned QuPath software uses a combination of image pre-processing to enhance cell boundaries, cell- and cell-boundary detection and image segmentation, supported by machine learning algorithms (Bankhead et al., 2017). Also inForm is a proprietary automated image analysis software package, which

provides tissue segmentation as well as cell segmentation algorithms for multiplex-stained images. Users manually annotate tissue categories for training, the software displays segmentation results and accuracy, allowing for iterative refinement. We have been using this software particularly for its tissue segmentation algorithm (van Wilpe et al., 2021; Bakkerus et al., 2024).

The cell segmentation-associated challenges have been resolved by the deep-learning-based ImmuNet algorithm developed to analyse the immune landscape in solid tumours (Sultan et al., 2023). ImmuNet is trained to identify the position and identity of cells. However, it is not a segmentation algorithm that splits the image into individual cells. By comparison, software packages such as QuPath or inForm segment the image into areas that are assigned to individual cells. Such algorithms carry a risk of over- and undersegmentation, thereby yielding erroneous cell numbers.

Regarding a number of similarities between cancer and endometriosis tissues in their cellular composition and tissue structure, endometriosis research should greatly benefit from the transfer of methods applied in the analysis of tumour tissue. Here, we developed a multiplex immunofluorescence (IF) panel targeting six markers of endometriosis-related tissue substructures. To visualize epithelium, stroma, and fibrosis, we used PanCK, CD10, and  $\alpha$ -SMA, respectively. Calretinin was used to identify mesothelial cells. CD45 was used as pan-immune marker, and Ki67 was used as proliferation marker.

With this at hand, we performed cell classification using an ImmuNet algorithm that had been trained on cancer tissue. Furthermore, we performed tissue segmentation with inForm to compare the proportions of epithelium, stroma, and fibrosis per sample, and to assess the immune-cell densities in these tissue substructures, comparing inForm and ImmuNet.

The results lay the foundation for a large-scale machine learning-based histological analysis of endometriotic lesions, to better understand and tackle heterogeneity within these subtypes.

## Materials and methods

### Ethical approval

The study protocol was assessed by the METC-Oost Nederland, medical ethics review committee and judged not to be subjected to the Dutch Act on Medical Research Involving Human Subjects.

### Human material

Endometriotic tissue was obtained from adult patients undergoing surgery for the treatment of suspected endometriosis. Tissue used for control IHC-stainings was provided from the Department of Pathology (Radboudumc, Nijmegen, The Netherlands) and obtained from patients undergoing surgery for other indications. Patients either did not opt-out from the research use of their tissue, if operated before April 2022, or if operated later provided informed consent.

### Preparation of histological sections

Sections of 4  $\mu$ m thickness were prepared from formalin-fixed paraffin-embedded (FFPE) tissue blocks. The sections were transferred on a floating water bath to stretch and minimize creases and captured on either normal glass (VWR, cat# 631-1553, China) for haematoxylin/eosin (HE) staining, or coated Superfrost glass (Eprelia, cat# J1800AMNZ, The Netherlands) for IHC and multiplex IF staining. After capturing, excess water was shaken off by hand and the slides were allowed to further drip off in a vertical position. Next, the slides were dried at 57°C for 1 h and subsequently dried at 37°C overnight.

## HE staining

HE stainings were performed manually. Sections were deparaffinized in two xylene (Scharlab, cat# XI00551000, Spain) baths for 5 min, followed by dipping in 3 baths of 99% ethanol (J.T. Baker, cat# 8025, Poland), followed by a running water bath. The slides were then stained in haematoxylin for 5 min, followed by 10 min running water bath, followed by 5 min eosin, and again rinsed for an instant in a running water bath. The slides were then dipped in three baths of 99% ethanol and two baths of xylene, and finally mounted with mounting medium (Tissue-Tek, cat# 1408, Poland).

## IHC-DAB

IHC with 3,3'-diaminobenzidine (DAB; Dako Omnis, cat# DM827, Singapore) was performed manually. Sections were deparaffinized as above. Next, the sections were subjected to endogenous peroxidase blocking for 10 min, using 3 wt% hydrogen peroxide (Boom, cat# 76051800.1000, The Netherlands) in Tris-buffered saline with Tween20 (TBST; Dako, cat# DM831, Singapore). Next, sections were rinsed in TBST for 10 min on a shaking plate. Heat-induced epitope retrieval (HIER) was performed using Tris/EDTA buffer (Dako Omnis, cat# DM848, Singapore) at pH 9. The sections were microwaved for 2.5 min at 800 W, followed by 10 min at 180 W. Next, the sections were rinsed in TBST for 5 min on a shaking plate. The sections were then surrounded by a hydrophobic PAP pen, and 150 µl of 1% bovine serum albumin in TBST were pipetted on the tissue for a pre-incubation of 10 min. The fluid was shaken off and the sections were incubated with the primary antibodies, at the respective dilutions (Table 1), for 60 min. All antibody incubations were conducted at room temperature in a dark, enclosed box. After fluid removal and rinsing, the sections were incubated with an anti-mouse and anti-rabbit secondary antibody (Dako Omnis, cat# SM802, Singapore) for 30 min. After rinsing, the DAB chromogen was applied, one drop per slide, and incubated for 10 min, followed by rinsing for 1 min in running water. Counterstaining was performed with haematoxylin for 30 s, followed by a running water bath. The sections were then dipped in three baths of 99% ethanol and two baths of xylene, and finally mounted with mounting medium.

## Manual immunofluorescence for monoplex stainings

Sections were deparaffinized as above. They were then washed in TBST for 2 min with agitation. HIER was performed as above, followed by washing with TBST for 2 min with agitation. The fluid was shaken off and the sections were surrounded by a hydrophobic PAP pen. Pre-incubation, antibody incubation, and subsequent rinsing were performed as stated above. The sections were then incubated with a secondary antibody (Akoya Biosciences,

Opal Polymer HRP, cat# ARH1001EA, USA) for 30 min. After rinsing for 10 min, 100 µl of the Opal 650 fluorophore (Akoya Biosciences, cat# FP1496001KT) was applied at 1/50 dilution for 10 min. The sections were rinsed and mounted with DAPI Fluoromount-G (SouthernBiotech, cat# 0100-20, USA), and dried in the dark.

## Automated immunofluorescence

Automated IF protocols were performed for the monoplex stainings with increasing number of HIER cycles as well as for the multiplex stainings with the finalized multiplex panel. For this, we employed the Opal 7-color Automation IHC Kit (Akoya Biosciences, cat# NEL871001KT) on the BOND RX IHC & ISH Research Platform (Leica Biosystems, USA) as described earlier (Gorris et al., 2023; Sultan et al., 2023). HIER was conducted using Bond Epitope Retrieval 2 (Leica Biosystems, AR9640) at 95°C for 20 min. Blocking was done using an antibody diluent (included in kit) for 10 min. Primary antibodies were incubated for 1 h and secondary antibodies for 30 min. The respective antibody to Opal fluorophore combinations are listed in Table 1. For the staining with PanCK combined with Opal 780 the slides were first incubated with the Opal TSA-DIG reagent for 10 min, then washed and then incubated with the Opal 780 fluorophore at 1/25 dilution for 60 min. Finally, the slides were counterstained with DAPI and mounted using Fluoromount-G (SouthernBiotech, cat# 0100-01, USA).

## Assessment of staining quality

The quality of the IF stainings was assessed for the similarity of the signal to the respective IHC-DAB stainings and the autoexposure time as a measure of staining intensity. The autoexposure time was measured using the Vectra Polaris 1.0 Automated Quantitative Pathology Imaging System (Akoya Biosciences).

## Image scanning and region of interest delineation

Images were scanned using the Vectra Polaris image scanner (Akoya Biosciences). Relevant region of interests (ROIs) were pre-selected based on HE stainings of the neighbouring serial section to contain only fibrotic tissue, endometriosis stroma, and endometriosis epithelium. Regions containing only fat cells or healthy tissue where endometriosis was growing onto, for example, normal ovarian or bowel structures, were excluded. For this purpose, on PhenoChart Whole Slide Viewer (Akoya Biosciences) ROIs were drawn, which were automatically divided into square tiles. Tiles including non-relevant parts like fat tissue were removed. Within the relevant ROI tiles, 3 to 12 tiles per slide were further used as training images to train the tissue- and

**Table 1.** Antibodies used for both immunohistochemistry-3,3'-diaminobenzidine (IHC-DAB) and immunofluorescence (IF) stainings, and their determined optimal dilution.

Antibody	Target	Clone	Brand	Country	DAB dilution	IF dilution	OPAL
Calretinin	Mesothelium	DAK-Calret1	Dako Omnis	SGP	1/100	1/400	520
CD10	End. stroma	56c6	Monosan	NLD	1/10	1/80	570
CD45	Pan-immune	2B11+PD7/26	Dako Omnis	SGP	1/250	1/2000	480
Ki67	Proliferation	MIB1	Dako Omnis	SGP	1/300	1/600	620
α-SMA	Myofibroblasts	1A4	Sigma Aldrich	DEU	1/30 000	1/240 000	690
PanCK	End. epithelium	AE1/AE3 + 5D3	Abcam	GBR	<sup>a</sup>	1/1000	780
CK7	End. epithelium	OV-TL-12/30	Cell Marque	DEU	1/800	<sup>b</sup>	<sup>b</sup>
Vimentin	End. stroma	V9	Klinipath	NLD	1/4000	<sup>c</sup>	<sup>c</sup>

The first six antibodies are listed in the order of the final multiplex panel.

<sup>a</sup> For PanCK, no IHC-DAB was performed.

<sup>b</sup> CK7 was replaced by PanCK for the IF stainings.

<sup>c</sup> Vimentin was dropped in favour of CD10 as stromal marker. End. = Endometriosis. Country codes compliant to ISO 3166.

cell-segmentation algorithms in the inForm 2.4—Tissue Finder Advanced Image Analysis Software (Akoya Biosciences).

### Tissue segmentation using inForm

We performed the tissue segmentation in inForm such that it would replicate the hierarchical tissue architecture of the glandular structures within endometriotic lesions. The analysis was hierarchical in the sense that a tissue substructure was assigned based on the dominant cell type. Four tissue categories were trained by successively providing manual annotations, assessing the segmentation over all training images, adding more annotations and retraining. The 'Blank' category was trained on cell-void background. The tissue segmenter was restricted to use only the components of DAPI, CD10,  $\alpha$ -SMA, and PanCK and autofluorescence, CD45, Calretinin and Ki67 were omitted to achieve a segmentation agnostic to these signals. The minimum segment size was set to 2000 pixels. This caused that any smaller segments that would be assigned to a given category, were assigned to the adjacent larger segment.

### Cell detection and identification using inForm

In inForm, the cell identification is performed in two steps, by an initial nucleus segmentation, followed by phenotyping of the assigned cell categories (Supplementary Fig. S1). Fine-tuning of the nucleus segmentation was achieved by limiting the relevant component to the DAPI counterstain, setting the relative nucleus intensity to 0.60, the splitting sensitivity to 0.20, the minimum nucleus size to 30 and the 'Fill Nuclear Holes' function to <30. Cell refinement after segmentation was not performed. To train the phenotype identification, a total of 110 CD45<sup>+</sup> and 110 other cells were manually annotated, across the bulk of all training images.

### Cell detection and identification using ImmuNet

ImmuNet is a segmentation free machine-learning algorithm which provides the cell location and phenotype, but no information about cell shape. It had been originally designed to phenotype immune cells in cell dense tissue environments, where other algorithms, including inForm tend to struggle (Sultan et al., 2023; van der Hoorn et al., 2024). The resulting data are similar to flow cytometry output, but with added spatial information and is indeed provided in Flow Cytometry Standard (FCS) format. It can therefore be analysed for marker (co-)expression or lack thereof and used to determine the abundance of cells of interest in the whole tissue, or when combined with tissue segmentation data, per tissue category.

Here we used an instance of the ImmuNet network (Gorris et al., 2022) specifically trained to recognize proliferation with Ki67 on lymphocytes (CD3<sup>+</sup> and CD20<sup>+</sup>) and tumour cells. To recognize CD45<sup>+</sup> cells in our samples we used the network's CD3 channel. Ki67 signal in our samples was recognized by the network's Ki67 channel. We used this network without any fine-tuning and being totally naïve to the endometriosis tissue to analyse our batch of nine samples. We then performed a manual gating on the identified cells to discern for CD45 and Ki67 positivity. This gating was then used on all nine samples to derive counts of CD45<sup>+</sup>/Ki67<sup>−</sup> as well as CD45<sup>+</sup>/Ki67<sup>+</sup> cells.

### Statistical analysis

The groups of four DE and OMA samples were compared by means of two-tailed t-test for either equal or unequal variances.

Equal variances were assumed if the factor of the greater to the lesser variance was <4.

## Results

The architecture of endometriosis lesions is commonly recognized as a composite of three tissue substructures, namely epithelium, stroma, and fibrotic tissue. In this work, we were interested in the proportions of these tissue substructures within endometriotic lesions, as well as the densities of immune cells and in particular proliferating cells in these areas.

Answering these two questions required the establishment of a multiplex IHC panel and a two-step machine learning-based image analysis. This protocol combined the segmentation of tissue subtypes by inForm, followed by the identification of immune cells by ImmuNet.

### IHC-DAB and multiplex panel

The multiplex panel was comprised of six cell-phenotypic markers along with the DAPI nuclear counterstain. The selection of antibodies was determined based on tissue subtypes within endometrial lesions. CD45 was included as a pan-immune marker and Ki67 for detection of proliferating cells (Table 1).

In multiplex IHC, antibodies are applied successively following heat-induced removal of the prior antibody. Since the resistance of epitopes to repeated heating may differ, the order of antibodies within the multiplex protocol has to be established as has the optimal dilution for each antibody (Gorris et al., 2018). We followed a stream-lined protocol which led us to the optimized panel via a well-defined standard operating procedure (Fig. 1). Initially, the staining intensity and specificity of all six antibodies were determined on both control tissues and a single deep endometriosis (DE) sample through IHC-DAB stainings. The final IHC-DAB stainings served as templates throughout all IF monoplex and multiplex stainings to visually assess their staining quality. The optimal antibody dilutions were found by closely comparing the stained DE sample with the respective control (Fig. 2) and adjusting the dilution and repeating the staining when necessary. Vimentin and CD10 are both common markers for endometriosis stroma. However, vimentin showed poor distinction between stroma and fibrotic tissue (Fig. 2). Therefore, we selected CD10 for our panel. CK7 is widely used to stain endometrial epithelium. Still, we decided to replace it by PanCK. This change was motivated by our earlier experience with the PanCK antibody, which we consistently use to visualize epithelium at 1/1000 dilution along with Opal 780 in other multiplex panels and which has to be used last in the multiplex procedure. There may be concerns that the PanCK also stains mesothelia. However, comparison of the IHC-DAB (Fig. 2) and pseudo-H-DAB (Supplementary Fig. S2) stainings demonstrates that PanCK is a viable alternative. Close inspection only showed some very minor overlap in some samples. However, we also found only little mesothelium in our samples. Thus, this particular choice may be worth revisiting in the future. For the remaining five antibodies, the optimal dilutions for IF were determined through repeated manual IF stainings, at increasing dilutions and using the Opal 650 fluorophore.

To determine the optimal incubation order, for each of the five antibodies (CD10,  $\alpha$ -SMA, calretinin, CD45, and Ki67) three staining sets were executed, subjected to either one, three, or five consecutive heating cycles, following the automated IF protocol.

Finally, for matching the used antibodies with the available Opal fluorophores, we drew upon previous experience within the



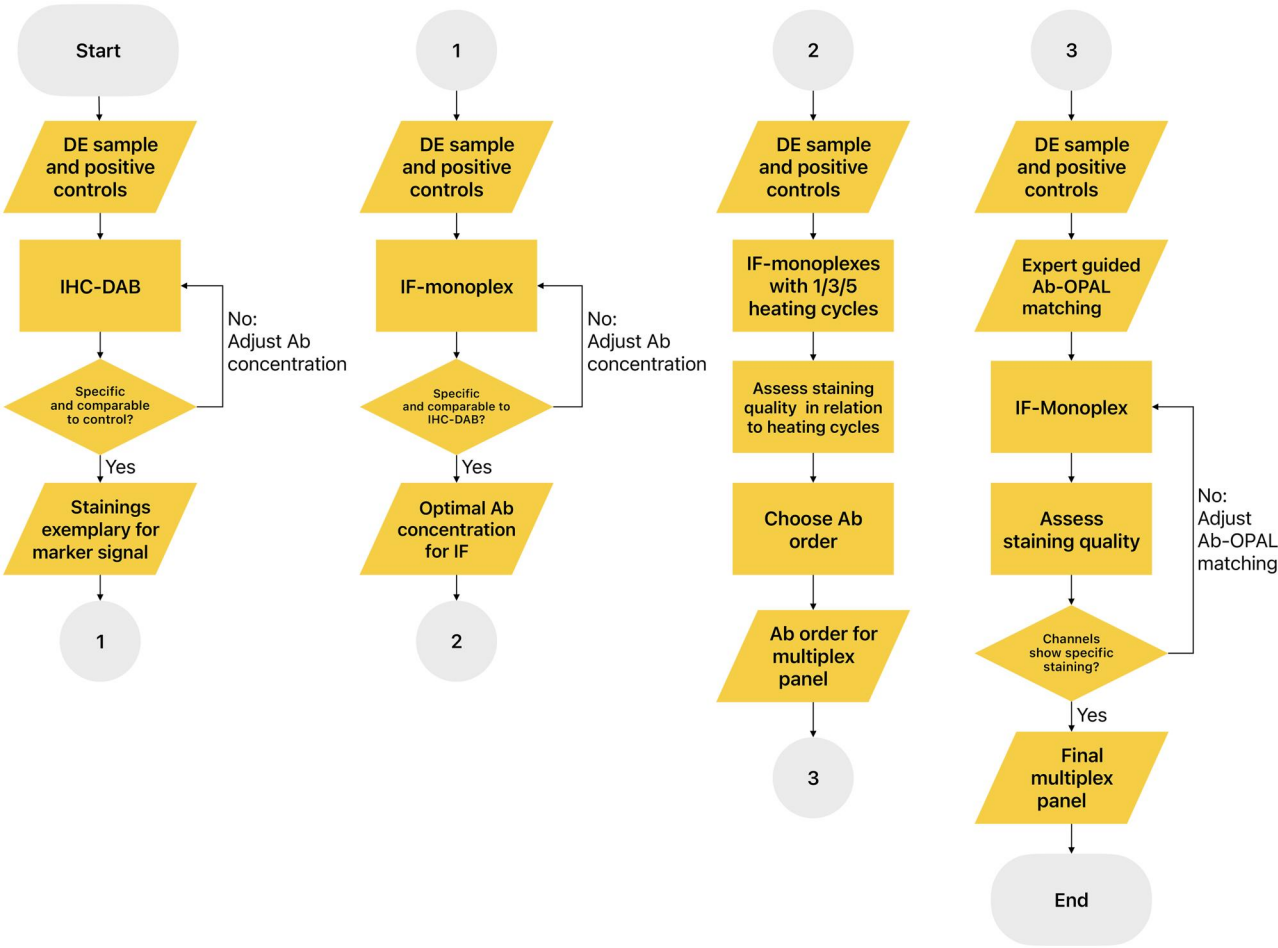


**Figure 1.** Flowchart summarizing the workflow in general terms, of creating and optimizing the 7-plex multiplex panel for endometriosis lesions. The final panel features PanCK, CD10,  $\alpha$ -SMA, calretinin, CD45, and Ki67 and uses DAPI as nuclear counterstain. Rhomboids depict in-/outputs. Rectangles depict operations. DE, deep endometriosis; IHC, immunohistochemistry; DAB = 3,3'-diaminobenzidine; Ab, antibody; IF, immunofluorescence; OPAL, opal fluorophores.

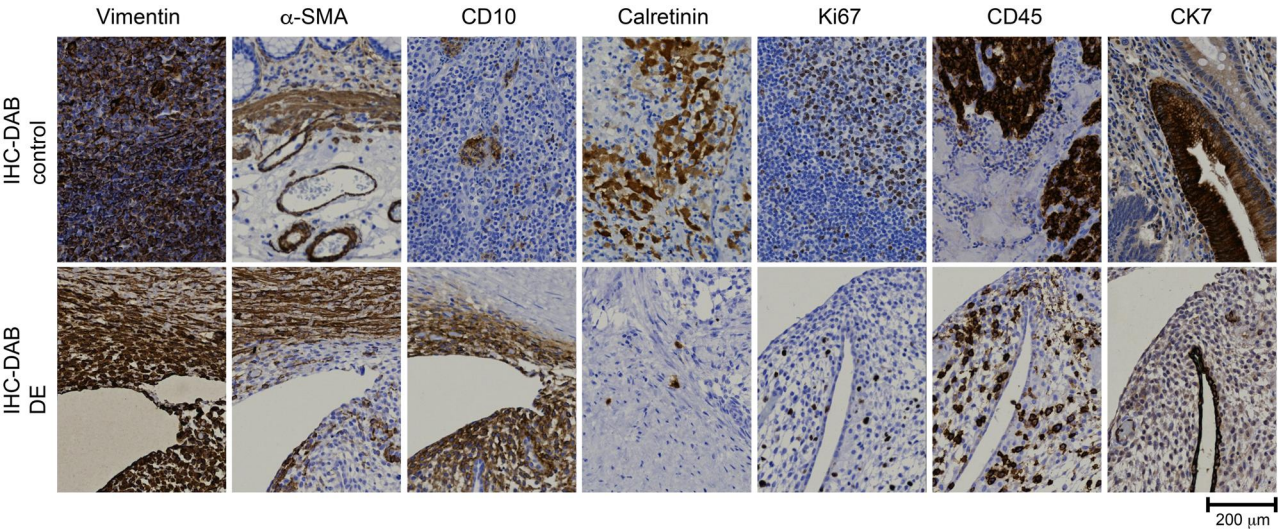


**Figure 2.** Overview of the IHC-DAB (immunohistochemistry—3,3'-diaminobenzidine) stainings for one deep endometriosis (DE) lesion. Control stainings were performed on mesothelioma for calretinin, colon for  $\alpha$ -SMA and CK7, and tonsil for the other targets.

research group. After an initial multiplex experiment, one subsequent adjustment was made, culminating in the final composition of the multiplex panel (Table 1, Fig. 3, Supplementary Fig. S2). With the finalized multiplex panel at hand, nine samples including four DE lesions, four OMA and one PE lesion were sectioned and stained with HE and the multiplex panel.

### Tissue segmentation

For tissue segmentation, we first defined our visual concept of an endometriotic lesion containing the main tissue subtypes of epithelium, stroma and fibrosis (Fig. 4). The cell-free lumen and the non-specifically stained background were assigned to the 'blank' category. For each histological section based on the multiplex staining, we made a manual pre-selection of the parts containing fibrotic tissue, endometriosis stroma and endometriosis epithelium that excluded approximately half of the tissue on the PE and DE lesions, whereas for the OMA lesions nearly the whole tissue was included (Supplementary Fig. S3).

Tissue segmentation was performed in inForm, by several iterations of annotating tissue and training the segmenter, up to an accuracy above 95%. This accuracy is reported automatically by inForm and indicates that the pixels in the training regions are classified with 95% accuracy.

The number of annotations that was required per category, to achieve this result was two for 'Blank', two for CD10<sup>+</sup> stroma, three for PanCK<sup>+</sup> epithelium and six for  $\alpha$ -SMA<sup>+</sup> tissue (Fig. 4). The subsequent tissue segmentation in inForm assigned areas of varying sizes to the 'blank' category, excluding them from the segmented tissue. As a consequence, the proportion of tissue that was available for segmentation for OMA was much larger than for DE and the PE lesion (Table 2, Supplementary Fig. S4).

### Cell identification

So far, the performance of cell identification of ImmuNet and inForm of 7-plex stains was compared on tumour tissue,

demonstrating the superior accuracy of ImmuNet (van der Hooft *et al.*, 2024). Here, the cell identification of ImmuNet was visually assessed for correct phenotyping and compared with the inForm phenotyping of CD45<sup>+</sup> cells. The procedure of cell segmentation in inForm is described in Supplementary Fig. S1. ImmuNet showed a satisfying phenotyping, whereas in line with van der

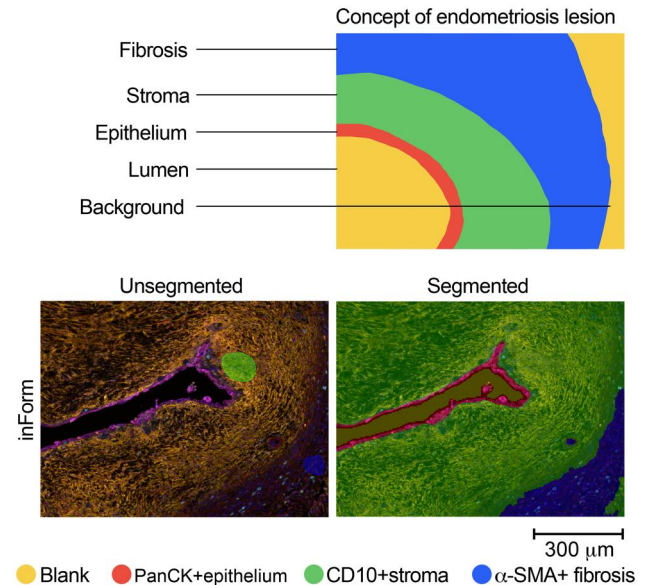


**Figure 4.** Concept of our understanding of an endometriosis lesion, and the derived tissue segmentation into three subtypes and the 'blank' category. Representative example of the automatic tissue segmentation in inForm. The bottom left picture shows manual annotations used as ground truth for training. The bottom right picture depicts the automated segmentation and assignment to the four tissue categories, blank = yellow, PanCK<sup>+</sup> epithelium = red, CD10<sup>+</sup> stroma = green,  $\alpha$ -SMA<sup>+</sup> tissue = blue.

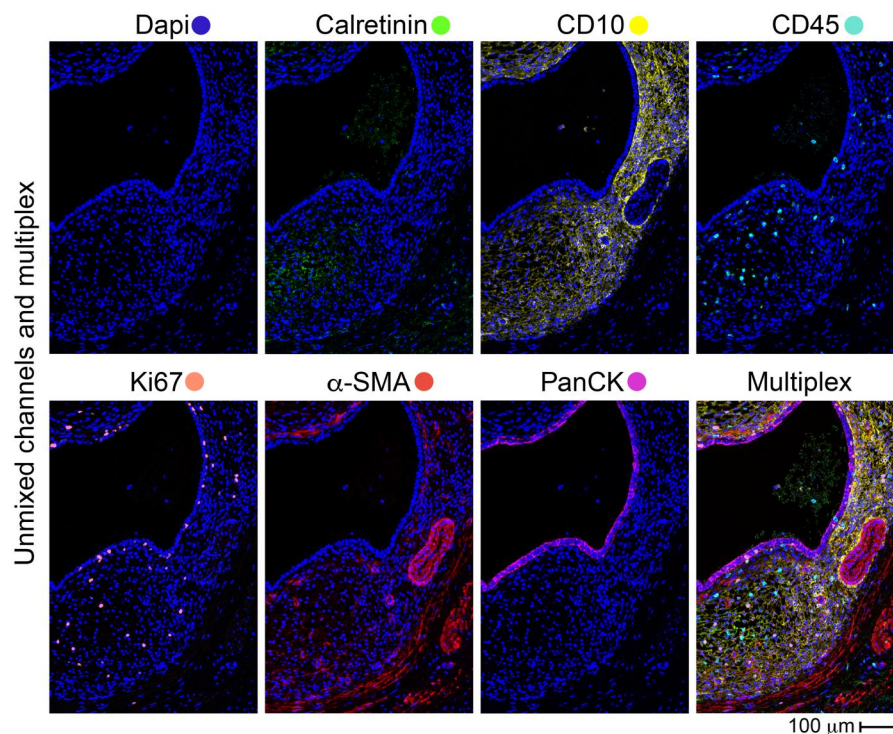


**Figure 3.** Multiplex staining of a deep endometriosis (DE) sample. Unmixed channels and complete multiplex image with colour scheme as indicated for the individual channels.



**Table 2.** Absolute areas of regions of interest (ROIs) and total segmented tissues (epithelium + stroma + fibrosis) in mm<sup>2</sup>.

Slide ID	DE 1	DE 2	DE 3	DE 4	OMA 1	OMA 2	OMA 3	OMA 4	PE 1
Total ROI area mm <sup>2</sup>	93.61	142.02	25.82	66.49	260.81	440.93	326.61	375.70	8.39
Total segmented tissue area mm <sup>2</sup>	75.77	76.87	9.35	33.77	177.95	357.37	261.26	219.35	2.10
% segmented tissue area	81%	54%	36%	51%	68%	79%	80%	65%	25%

DE, deep lesions; OMA, ovarian endometrioma; PE, superficial peritoneal.

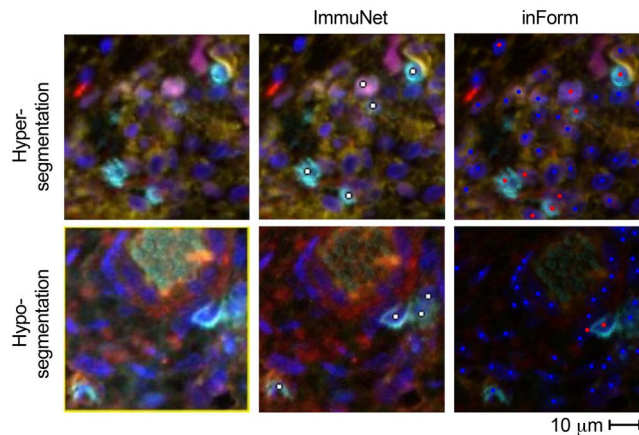


**Figure 5.** Comparison of identification of CD45<sup>+</sup> cells (cyan) with ImmuNet and inForm. CD45<sup>+</sup> cells identified in ImmuNet are indicated by white dots, in inForm by red dots; other cells identified by inForm are indicated by blue dots. Examples of areas in which inForm yields hyper- and hyposegmentation respectively, in comparison to ImmuNet.

Hoom et al. (2024) inForm showed hypersegmentation (identifying more cells than visible) as well as hyposegmentation (failing to identify visible cells) (Fig. 5). Overall, the image analysis workflow was developed and compared against other options along a well-defined procedure (Fig. 6).

Segmentation data analysis

Finally, we applied the integrated workflow to extract the number of immune cells (CD45<sup>+</sup>) and the fraction of proliferating immune cells (CD45<sup>+</sup>/Ki67<sup>+</sup>) for the various tissue subtypes. The ImmuNet cell identifications for all CD45<sup>+</sup> immune cells and the part of Ki67<sup>+</sup> cells were obtained using an ImmuNet instance trained on tumour tissue, without any further fine-tuning on endometriosis tissue. Combined with the tissue segmentation data from inForm the densities of cells for the total lesions and per tissue category could be analysed. In spite of the limited size of the data set, the difference between the groups of DE and OMA lesions was tested for significance. To determine whether equal or unequal variances should be assumed the ratio of variances was calculated. A ratio below 4 indicated the presence of equal variances. The lowest *P*-value of 0.11 was found for the proportion of epithelium, which was higher in deep endometriosis lesions in comparison to endometrioma. Except for one DE sample, all lesions were composed of more than 60% fibrotic tissue. The fraction of fibrotic tissue and epithelium showed a relatively small variation amongst the OMA lesions. All other percentages varied considerably across the individual samples (Fig. 7). For the OMA lesions, the density of CD45<sup>+</sup> cells in fibrotic tissue was similar to the total density, which is in line with the high fibrotic tissue content. DE and OMA lesions also showed a similar content of CD45<sup>+</sup> cells in epithelium. What stands out is the relatively high proportion of Ki67-positive CD45<sup>+</sup> cells in the epithelium

and stroma of OMA lesions. Overall, the fraction of proliferating CD45 cells was highest in epithelium (Fig. 8).

Discussion

In this pioneering study, we introduced the combination of multiplex staining and machine-learning-based tissue segmentation and cell identification to endometriosis research using a panel of samples that covered the prominent lesion types. Cell detection was performed with the ImmuNet algorithm, a deep learning AI image algorithm that was trained on multiplex images of tumours. No further training was performed for application to the endometriosis samples which is denoted as a zero-shot approach. At the same time, we present a fully optimized multiplex panel that reports on the most important cells in endometriotic lesions. Implementation of the antibody panel and validation of the image analysis workflow proceeded along well-defined workflows (Figs 1 and 6).

In the clinical presentation of endometriosis, which is predominantly a disease presenting with dysmenorrhoea, chronic pelvic pain, and/or subfertility, fibrosis is a key pathological component, influencing both the tissue structure and progression of lesions. Fibrotic tissue, driven by myofibroblast activity and excessive collagen deposition, has been proposed to lead to entrapment of nerves, causing the chronic pain associated with the condition (Visser et al., 2024). Thus, not only the presence of epithelial and stromal cells but also fibrotic tissue seems to be a prerequisite in the formation of clinically relevant endometriosis.

The machine learning-based tissue segmentation approach based on multiplex IHC we explored here provides a complementary avenue to analyse the distribution and severity of fibrosis in endometriotic lesions. By accurately segmenting fibrotic regions and identifying cell types within these areas, this technique has the potential to achieve insights that can inform therapeutic approaches for managing chronic pain and the impact fibrosis in endometriosis has on fertility. Further developments, including the implementation of additional markers and more fine-grained tissue segmentation approaches, can leverage the potential of this technology in endometriosis even further in the future.

The protocol we used for multiplex staining validated antibody dilutions, matching of fluorophores and the optimal sequence of successive antibody incubations. To visualize endometriosis stroma, we initially compared vimentin with CD10. Vimentin had been used early in endometriosis research (Nisolle et al., 1995; Klemmt et al., 2006) but has since been succeeded by CD10 (Arafah et al., 2021; Bergman-Larsson et al., 2022) because of its higher specificity for endometrial stromal cells. Our comparison confirmed this notion and supported the choice for CD10 (Fig. 2). CK7 is an established marker for endometrial epithelium (Jiang et al., 2013; Istrate-Ofiteru et al., 2022). PanCK is a broad spectrum cytokeratin marker containing the monoclonal AE1/AE3 and 5D3 antibodies, of which the latter also stains CK7 (Lin et al., 2011) and thus endometrial epithelium (Fig. 3). We decided to replace CK7 for PanCK because of our group's experience with these antibodies

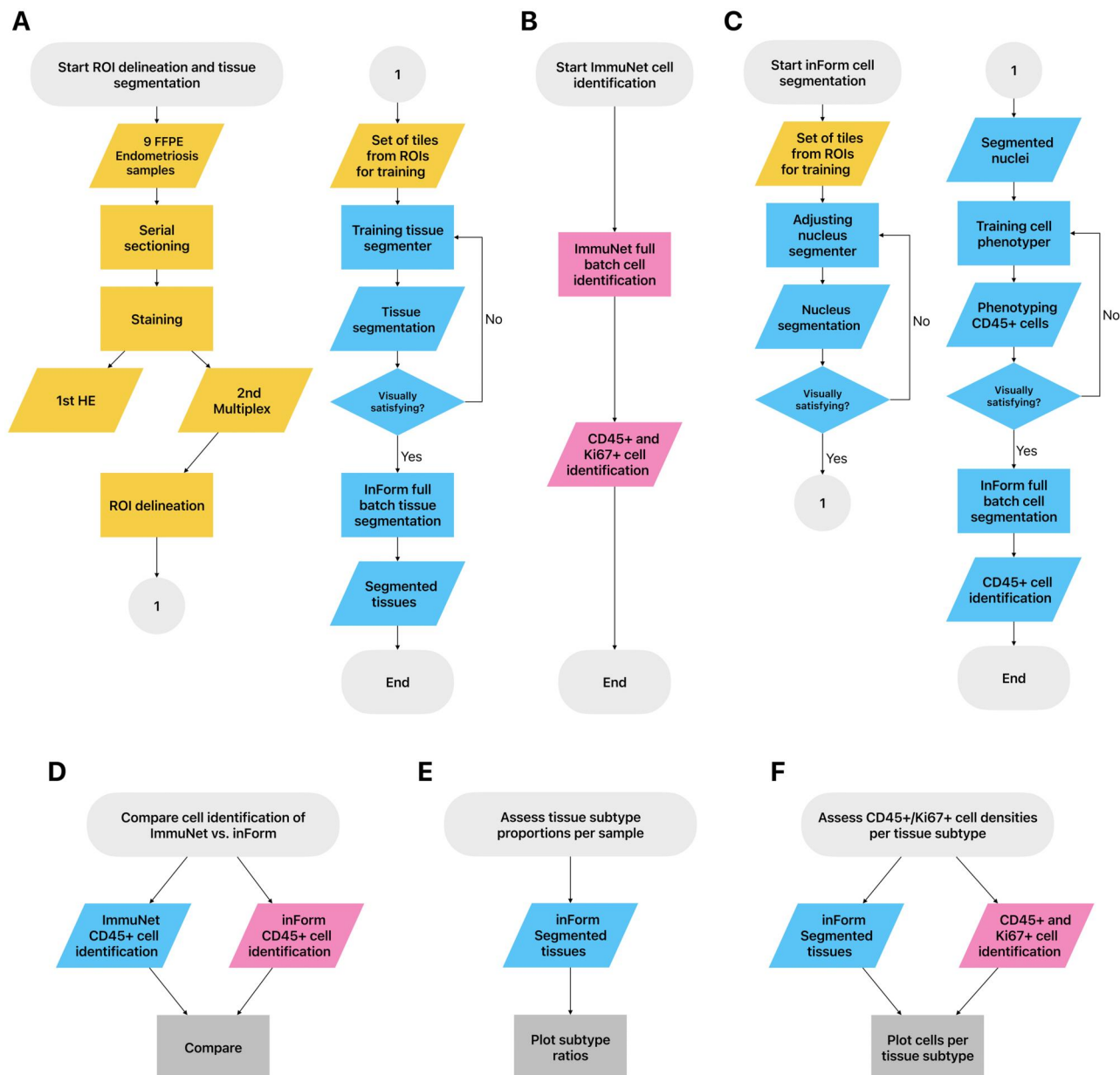


**Figure 6.** Flowchart summarizing the workflow starting from the nine endometriosis formalin-fixed paraffin-embedded (FFPE) samples to the final tissue segmentation and cell identification using InForm, and ImmuNet. The ImmuNet cell identification was compared to that of InForm. The InForm tissue segmentation was used to assess the proportion of tissue subtypes per lesions, and also combined with ImmuNet's cell identification to derive cell densities per tissue subtype. Rhomboids depict in-/outputs. Rectangles depict operations. Diamonds depict decision points. Colour codes correspond to the mode of processes, yellow = manual, blue = InForm, magenta = ImmuNet.

in other multiplex panels (van der Woude et al., 2022). As detailed above, we only observed very little overlap of calretinin and PanCK-positive structures. Thus, we consider this decision a valid choice.

A subset of our panel, complemented with markers to probe for lymph vessels and vascularization was employed for multiplex IHC of endometrium and myometrium of patients with adenomyosis (Harmsen et al., 2022). In addition to demonstrating the value of simultaneous quantification of key tissue structures, the combination of tissue segmentation with cell identification, as conducted here, provides a deeper understanding of cell densities in relation to tissue substructure as demonstrated for dividing immune cells.

The analysis of the stained and scanned samples started with the manual selection of ROIs that only contained glandular

structures comprising epithelium and stroma, and adjacent fibrosis. This pre-selection was useful as it allowed for the categorization of all  $\alpha$ -SMA<sup>+</sup> tissue, surrounding CD10<sup>+</sup> and PanCK<sup>+</sup> tissue, as fibrosis. An alternative would be to add more tissue categories to the tissue segmenter to capture any irrelevant tissue fragments that would not fit into the three categories, plus the 'blank' category. However, this approach proved to be difficult as adding more than four tissue categories exceeded the available computing power during training of the InForm segmenter. In the future, it will be important to further define standards on how to perform the manual pre-selection. Histological sections of endometriosis lesions are very heterogeneous and the proportion of epithelium to stroma to fibrotic tissue can vary strongly. We manually preselected those parts of the sections that contained fibrotic tissue, endometriosis stroma and endometriosis



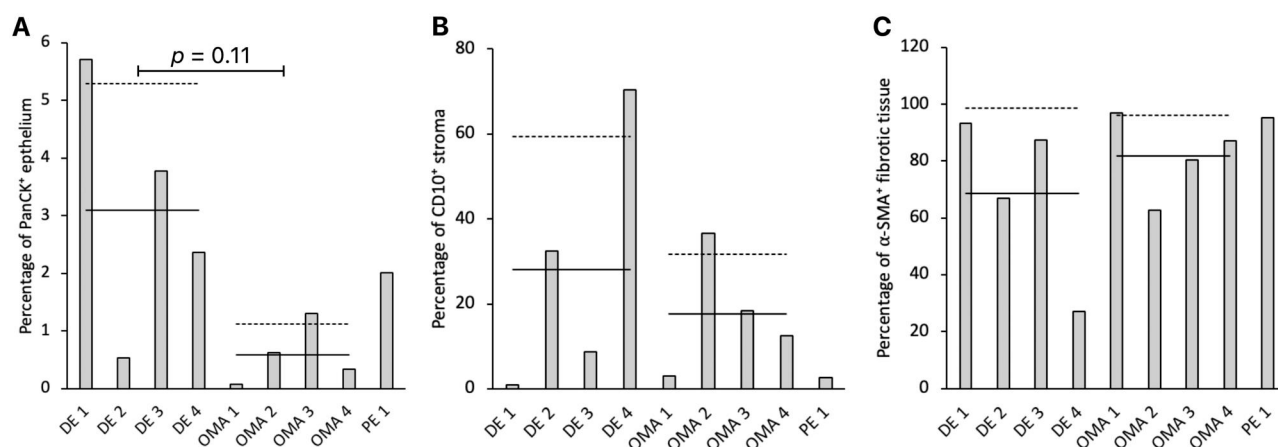


**Figure 7.** Percentage of tissue compartment areas of the total segmented areas for all nine samples. (A) Epithelium as determined by PanCK staining, (B) stroma as determined by CD10 staining, and (C) fibrotic tissue as determined by  $\alpha$ -SMA staining. Solid lines indicate mean, dashed lines indicate upper standard deviation, combined for the DE and OMA samples. Two-tailed t-test for unequal variances performed for all three graphs. The lowest found P-value is reported.

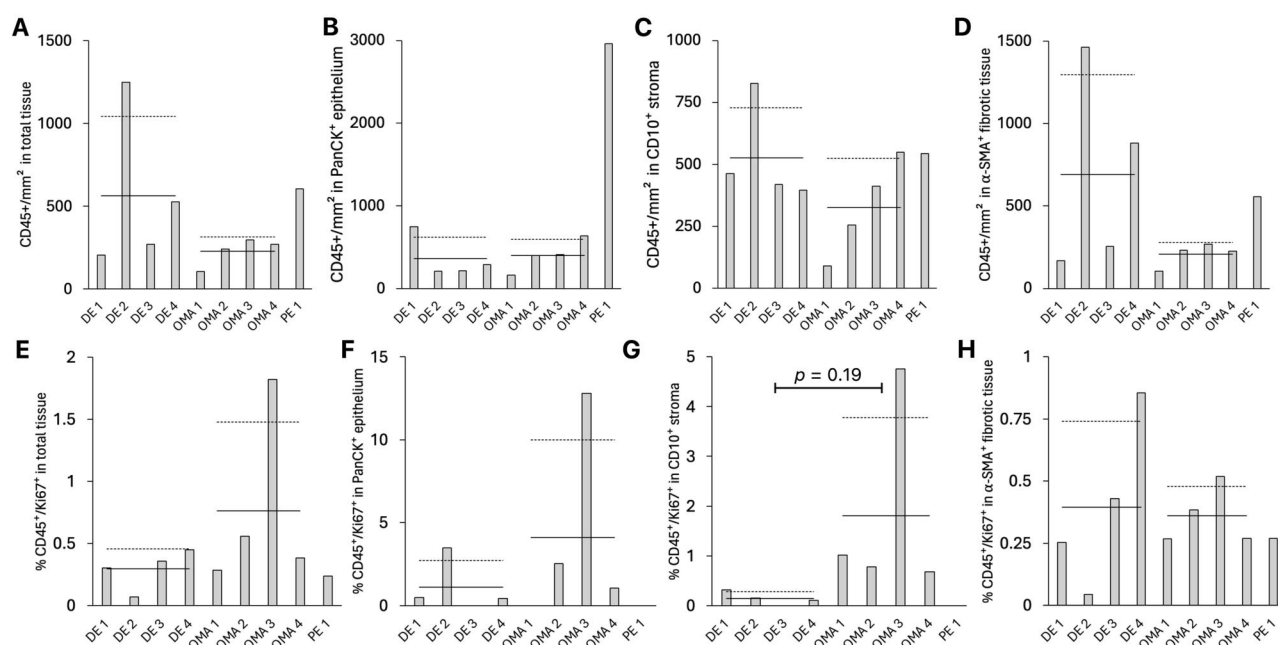


**Figure 8.** Immune cell densities and percentages. (A–D) Densities of CD45<sup>+</sup> immune cells in (A) total tissue, (B) PanCK-positive epithelium, (C) CD10-positive stroma, and (D)  $\alpha$ -SMA-positive fibrotic tissue. (E–H) Percentages of CD45<sup>+</sup>/Ki67<sup>+</sup> proliferating immune cells in (E) total tissue, (F) PanCK-positive epithelium, (G) CD10-positive stroma, and (H)  $\alpha$ -SMA-positive fibrotic tissue. Solid line indicates mean, dashed line indicates upper standard deviation, combined for the DE and OMA samples. t-test had been performed to compare DE and OMA groups in all graphs. The lowest found P-value is reported.

epithelium, thereby excluding fatty tissue. Given the heterogeneity of lesions in terms of size, which is further affected by processing during acquisition of the biopsy and histological procedures, analyses with respect to cell numbers per area per tissue type are more informative than total cell counts (McKinnon et al., 2022).

One drawback on relying on the cytosolic  $\alpha$ -SMA signal for fibrosis segmentation was the presence of unstained perforations in cell sparse parts that originally contained collagen deposits. These areas tended to be assigned to the 'blank' category, trained on cell void background (Supplementary Fig. S5). Fibrosis is characterized by  $\alpha$ -SMA<sup>+</sup> myofibroblasts that produce collagen at a rate exceeding its breakdown. In endometriosis, this collagen production proceeds in the absence of intervention (Huang et al.,

2022). Fibrotic regions can increase in collagen and other extracellular matrix proteins over time (Wynn, 2007). It is therefore possible that the area of such blank spaces might correlate with lesion age or severity of symptoms (Odagiri et al., 2009; Zhang et al., 2016).

Future developments should thus aim to also quantitate these tissue parts. Possibilities could be (i) the inclusion of a collagen marker in the panel or (ii) a collagen-specific Masson's trichrome staining of an adjacent section to derive the fibrosis outline.

We saw that after tissue segmentation, the combined tissue areas of epithelium, stroma and fibrosis, were less amongst the DE and PE lesions (Table 2). This means that effectively less tissue was available for the consecutive cell identification, compared to the OMA lesions. This could be attributed to a higher

amount of fat tissue within the DE and PE lesions, which laid within the selected ROIs and hence was not removed during the manual pre-selection.

In the analysis of CD45<sup>+</sup> cell density, the DE2 lesion spiked out with a high density in the total and fibrotic tissue (Fig. 8). At closer examination of the staining, we observed several CD45<sup>+</sup> cell-dense nodes, resembling tertiary follicular structures (TLS). However, the density of proliferative Ki67<sup>+</sup>/CD45<sup>+</sup> cells was the lowest in the DE2 lesion (Fig. 8).

The observation of TLS in an endometriotic lesion has been reported earlier. TLS are composed of B- and T-cells (Tan et al., 2022). For a better understanding and comparison between lesions, it might be beneficial to regard TLS and infiltrating immune cells separately. This could be achieved by filtering out TLS from the multiplex image using the CD45 channel, for example by including a separate category for high-density CD45<sup>+</sup> regions, before continuing with the tissue and cell segmentation.

In this study, we were interested in distinguishing the main histological structures of endometriosis lesions. Future studies should zoom in more on the frequency and distribution of various immune cells. We will particularly be interested in addressing macrophage (subsets) as these have been implicated in the progression as well as resolution of fibrotic changes (Gorris et al., 2023).

The ImmuNet cell segmentation was performed using a version that was previously trained to recognize immune cells in tumours, stained with a different antibody panel. No additional training was performed, meaning that the network was naïve to our endometriosis samples. The ability of ImmuNet to perform cell phenotyping on tissue types that were not part of its training set underlines the potential of the method for heterogenous endometriosis samples.

The fundamental superiority of ImmuNet above inForm, in the accuracy of cell detection has been proven earlier in the work of van der Hoorn (van der Hoorn et al., 2024). Based on this, we visually assessed ImmuNet's performance on our stainings.

Taken together, we have taken the first step in the combination of multiplex staining with machine learning-based cell detection in endometriosis research. Starting from the solid base of our optimized multiplex panel we were able to distinguish main tissue subtypes and perform a quantification of cells within these areas. Furthermore, we gained valuable insights for future refinements of the presented protocol such as specific identification of collagen-rich structures and tertiary follicular structures.

## Supplementary data

Supplementary data are available at *Human Reproduction* online.

## Data availability

The data underlying this article will be shared on reasonable request to the corresponding author.

## Acknowledgements

We thank Evgenia Martynova, Iris van der Hoorn, and Mark Sweep from the Medical BioSciences department at Radboudumc, for their help in setting up the cell phenotyping with ImmuNet. We thank Francesco Ciompi from the Computational Pathology Group at Radboudumc for his advice in the early beginning of our

project. We also thank the Radboudumc Technology Center Microscopy for use of their microscopy facilities.

## Authors' roles

S.E.K. and M.A.J.G. established the multiplex IHC workflow and performed the image analysis. G.V. processed and selected endometriosis samples. K.V. helped with the multiplex IHC analysis. M.S. provided gynaecopathological expertise. A.W.N. provided expertise on endometriosis. W.P.R.V., G.V. and A.W.N. provided expertise on fibrosis in endometriosis. S.T., M.S., and R.B. conceptualised the study. S.E.K. wrote the initial draft of the manuscript. R.B., M.S., S.T., M.A.J.G., and A.W.N. revised the manuscript. All authors read and approved the manuscript.

## Funding

The study was funded by the departments of Medical BioSciences and Gynecology and Obstetrics of the Radboudumc, Nijmegen, The Netherlands.

## Conflict of interest

The authors do not declare any competing interests.

## References

- Arafah M, Rashid S, Akhtar M. Endometriosis: a comprehensive review. *Adv Anat Pathol* 2021;**28**:30–43.
- Asante A, Taylor RN. Endometriosis: the role of neuroangiogenesis. *Annu Rev Physiol* 2011;**73**:163–182.
- Bakkerus L, Subtil B, Bontkes HJ, Gootjes EC, Reijm M, Vullings M, Verrijp K, Bokhorst JM, Woortman C, Nagtegaal ID et al. Exploring immune status in peripheral blood and tumor tissue in association with survival in patients with multi-organ metastatic colorectal cancer. *Oncoimmunology* 2024;**13**:2361971.
- Bankhead P, Loughrey MB, Fernandez JA, Dombrowski Y, McArt DG, Dunne PD, McQuaid S, Gray RT, Murray LJ, Coleman HG et al. QuPath: open source software for digital pathology image analysis. *Sci Rep* 2017;**7**:16878.
- Bergman-Larsson J, Gustafsson S, Mear L, Huvila J, Tolf A, Olovsson M, Ponten F, Edqvist PD. Combined expression of HOXA11 and CD10 identifies endometriosis versus normal tissue and tumors. *Ann Diagn Pathol* 2022;**56**:151870.
- Chung MS, Han SJ. Endometriosis-associated angiogenesis and anti-angiogenic therapy for endometriosis. *Front Glob Womens Health* 2022;**3**:856316.
- Colgrave EM, Keast JR, Bittinger S, Healey M, Rogers PAW, Holdsworth-Carson SJ, Girling JE. Comparing endometriotic lesions with eutopic endometrium: time to shift focus? *Hum Reprod* 2021;**36**:2814–2823.
- Gorris MAJ, Halilovic A, Rabold K, van Duffelen A, Wickramasinghe IN, Verweij D, Wortel IMN, Textor JC, de Vries IJM, Figdor CG. Eight-color multiplex immunohistochemistry for simultaneous detection of multiple immune checkpoint molecules within the tumor microenvironment. *J Immunol* 2018;**200**:347–354.
- Gorris MAJ, Martynova E, Sweep MWD, van der Hoorn IAE, Sultan S, Claassens M, van der Woude LL, Verrijp K, Figdor CG, Textor J et al. Multiplex immunohistochemical analysis of the spatial immune cell landscape of the tumor microenvironment. *J Vis Exp* 2023;**198**:e65717.
- Gorris MAJ, van der Woude LL, Kroeze LI, Bol K, Verrijp K, Amir AL, Meek J, Textor J, Figdor CG, de Vries IJM. Paired primary and

- metastatic lesions of patients with ipilimumab-treated melanoma: high variation in lymphocyte infiltration and HLA-ABC expression whereas tumor mutational load is similar and correlates with clinical outcome. *J Immunother Cancer* 2022;**10**:e004329.
- Harmsen MJ, Arduc A, Bleeker MCG, Juffermans LJM, Griffioen AW, Jordanova ES, Huirne JAF. Increased Angiogenesis and Lymphangiogenesis in Adenomyosis Visualized by Multiplex Immunohistochemistry. *Int J Mol Sci* 2022;**23**:8434.
- Horne AW, Missmer SA. Pathophysiology, diagnosis, and management of endometriosis. *BMJ* 2022;**379**:e070750.
- Huang Q, Liu X, Guo SW. Higher fibrotic content of endometriotic lesions is associated with diminished prostaglandin E2 signaling. *Reprod Med Biol* 2022;**21**:e12423.
- Istrate-Ofițeru A-M, Berbecaru E-I-A, Zorilă G-L, Roșu G-C, Diră LM, Comănescu CM, Drăgușin RC, Ruican D, Nagy RD, Iliescu DG et al. Specific local predictors that reflect the tropism of endometriosis—a multiple immunohistochemistry technique. *Int J Mol Sci* 2022;**23**:5614.
- Jiang W, Roma AA, Lai K, Carver P, Xiao SY, Liu X. Endometriosis involving the mucosa of the intestinal tract: a clinicopathologic study of 15 cases. *Mod Pathol* 2013;**26**:1270–1278.
- Kalaitzopoulos DR, Samartzis N, Kolovos GN, Mareti E, Samartzis EP, Eberhard M, Dinas K, Daniilidis A. Treatment of endometriosis: a review with comparison of 8 guidelines. *BMC Womens Health* 2021;**21**:397.
- Klemmt PA, Carver JG, Kennedy SH, Koninckx PR, Mardon HJ. Stromal cells from endometriotic lesions and endometrium from women with endometriosis have reduced decidualization capacity. *Fertil Steril* 2006;**85**:564–572.
- Laschke MW, Menger MD. Basic mechanisms of vascularization in endometriosis and their clinical implications. *Hum Reprod Update* 2018;**24**:207–224.
- Lin WL, Chen FL, Han CP. Anti-cytokeratin CAM5.2 (BD Biosciences) and CK8 give no remarkable advantages to the pancytokeratin cocktail of antibodies (AE1/AE3, CAM5.2, MNF116, CK8, and CK18) in detecting disseminated tumor cells in biologic subtypes of stage I-III breast cancer patients. *Ann Surg Oncol* 2011;**18**:S261–262. Author reply S263–S264.
- Machairiotis N, Stylianaki A, Dryllis G, Zarogoulidis P, Kouroutou P, Tsiamis N, Katsikogiannis N, Sarika E, Courcotsakis N, Tsiouda T et al. Extrapelvic endometriosis: a rare entity or an under diagnosed condition? *Diagn Pathol* 2013;**8**:194.
- McKinnon BD, Nirgianakis K, Ma L, Wotzkow CA, Steiner S, Blank F, Mueller MD. Computer-aided histopathological characterisation of endometriosis lesions. *J Pers Med* 2022;**12**:1519.
- Nisolle M, Casanas-Roux F, Donnez J. Coexpression of cytokeratin and vimentin in eutopic endometrium and endometriosis throughout the menstrual cycle: evaluation by a computerized method. *Fertil Steril* 1995;**64**:69–75.
- Odagiri K, Konno R, Fujiwara H, Netsu S, Yang C, Suzuki M. Smooth muscle metaplasia and innervation in interstitium of endometriotic lesions related to pain. *Fertil Steril* 2009;**92**:1525–1531.
- Raffi L, Suresh R, McCalmont TH, Twigg AR. Cutaneous endometriosis. *Int J Womens Dermatol* 2019;**5**:384–386.
- Rojas F, Hernandez S, Lazcano R, Laberiano-Fernandez C, Parra ER. Multiplex immunofluorescence and the digital image analysis workflow for evaluation of the tumor immune environment in translational research. *Front Oncol* 2022;**12**:889886.
- Sultan S, Gorris MAJ, Martynova E, van der Woude LL, Buytenhuijs F, van Wilpe S, Verrijp K, Figdor CG, de Vries IJM, Textor J. ImmuNet: a segmentation-free machine learning pipeline for immune landscape phenotyping in tumors by multiplex imaging. *bioRxiv*. <https://doi.org/10.1101/2021.10.22.464548>, 2023, preprint: not peer reviewed.
- Tan Y, Flynn WF, Sivajothi S, Luo D, Bozal SB, Dave M, Luciano AA, Robson P, Luciano DE, Courtois ET. Single-cell analysis of endometriosis reveals a coordinated transcriptional programme driving immunotolerance and angiogenesis across eutopic and ectopic tissues. *Nat Cell Biol* 2022;**24**:1306–1318.
- van Dam S, Baars MJD, Vercoulen Y. Multiplex tissue imaging: spatial revelations in the tumor microenvironment. *Cancers (Basel)* 2022;**14**:3170.
- van der Hoorn IAE, Martynova E, Subtil B, Meek J, Verrijp K, Textor J, Florez-Grau G, Piet B, van den Heuvel MM, de Vries IJM et al. Detection of dendritic cell subsets in the tumor microenvironment by multiplex immunohistochemistry. *Eur J Immunol* 2024;**54**:e2350616.
- van der Woude LL, Gorris MAJ, Wortel IMN, Creemers JHA, Verrijp K, Monkhorst K, Grünberg K, van den Heuvel MM, Textor J, Figdor CG et al. Tumor microenvironment shows an immunological abscopal effect in patients with NSCLC treated with pembrolizumab-radiotherapy combination. *J Immunother Cancer* 2022;**10**:e005248.
- van Wilpe S, Gorris MAJ, van der Woude LL, Sultan S, Koornstra RHT, van der Heijden AG, Gerritsen WR, Simons M, de Vries IJM, Mehra N. Spatial and temporal heterogeneity of tumor-infiltrating lymphocytes in advanced urothelial cancer. *Front Immunol* 2021;**12**:802877.
- Vissers G, Giacomozzi M, Verdurmen W, Peek R, Nap A. The role of fibrosis in endometriosis: a systematic review. *Hum Reprod Update* 2024;**30**:706–750.
- Wynn TA. Common and unique mechanisms regulate fibrosis in various fibroproliferative diseases. *J Clin Invest* 2007;**117**:524–529.
- Zhang Q, Duan J, Olson M, Fazleabas A, Guo SW. Cellular changes consistent with epithelial-mesenchymal transition and fibroblast-to-myofibroblast transdifferentiation in the progression of experimental endometriosis in baboons. *Reprod Sci* 2016;**23**:1409–1421.
- Zidane M, Makky A, Bruhns M, Rochwarger A, Babaei S, Claassen M, Schurch CM. A review on deep learning applications in highly multiplexed tissue imaging data analysis. *Front Bioinform* 2023;**3**:1159381.



© The Author(s) 2024. Published by Oxford University Press on behalf of European Society of Human Reproduction and Embryology.  
This is an Open Access article distributed under the terms of the Creative Commons Attribution-NonCommercial License (<https://creativecommons.org/licenses/by-nc/4.0/>), which permits non-commercial re-use, distribution, and reproduction in any medium, provided the original work is properly cited. For commercial re-use, please contact [reprints@oup.com](mailto:reprints@oup.com) for reprints and translation rights for reprints. All other permissions can be obtained through our RightsLink service via the Permissions link on the article page on our site—for further information please contact journals.permissions@oup.com.  
Human Reproduction, 2025, 40, 450–460  
<https://doi.org/10.1093/humrep/deae267>  
Original Article